

Rate of quantum tunnelling measured in a cold ion-molecule reaction

Charles Yang

May 24, 2024

1 Astrophysical motivation

The hydride anion, H^- , is suspected to exist in the interstellar medium (ISM) and have played an important role in stellar formation. In particular, it likely is the original source of molecular hydrogen, before dust grains allowed surface chemistry, through the pathway[1]



This is because three-body collisions are heavily suppressed by low densities while vibrational/rotational transitions are dipole forbidden due to no transition/permanent dipole moment respectively[2]. Its presence can also help to explain the observation of the cyanide anion CN^- in the ISM. Rate calculations for radiative electron attachment are too slow to explain the concentration observed in the ISM[3]**TODO: Check this is true** However, the pathway proposed in**TODO: when I have vpn access** can help to explain the observation of cyanide:



since hydrogen cyanide is produced in stellar ejecta[4].

In general, it is very difficult to observe anionic species in the ISM, as UV radiation fields can very easily remove the extra electron. To this point, the hydride anion has only a single bound state at 0.77 eV, and thus has no spectral lines which can be used as a convincing marker. Rather, the species H_3^- could be used as a tracer[5] due to its IR vibrotational spectrum. Supposing this species will be eventually observed with high enough sensitivity, its chemistry can be used to probe the amount of H^- in the ISM.

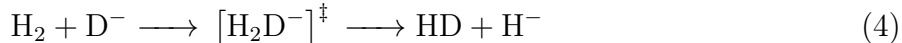
2 Chemistry

The reaction that allows this is



TODO: Figure out why this isn't studied, probably from [6], that the low potential well means that the molecule can easily be broken apart.

While H_3^- has a binding energy of 13 meV, which means it can in principle be isolated at $\lesssim 150$ K it is easier instead to consider the analogue



since the heavier mass of deuterium decreases the vibrational zero point energy of the products on the RHS, driving the reaction forward through a release of energy. However, electrically, H^- and D^- are almost identical, and so we expect the attack on the LHS to be very similar to Eq. 3. Furthermore, it is much easier to measure the rate of this reaction, since the end products don't back-react to recreate the starting material, and all anionic species can very easily be separated by their charge-to-mass ratio by either time of flight or cyclotron radius. Combined, these two features make the determination of the rate constant significantly easier.

In particular **TODO: something about photo deionization and cold**. In particular, the environment of the ISM is very sparsely populated and cold, so **TODO: idk lol**. In such conditions, given the experimentally determined reaction barrier of about 330 meV [7], the reaction can only proceed incredibly slowly via tunnelling. Estimates for an upper bound on the reaction rate by [8] indicated the need for both high concentrations and long reaction times in able to obtain the necessary reaction rates.

Para vs ortho, 21 cm line as spin-flip leads to $k_B T \sim 1$ K [2]

3 Benchmarking Quantum Theory

Furthermore, as this reaction proceeds chiefly through quantum tunnelling, it can be used as a valuable test of quantum theories and ab initio calculations. As arguably the simplest possible reaction with the simplest possible reactants, the reaction 4 is one of the simplest to treat theoretically. Numerous analyses are available using different computation schemes

4 Experiment

4.1 Manipulating and Measuring Ions

4.1.1 Electrostatics and Wiley-Maclauren spectrometer

Naturally, as charged particles, ions can be manipulated using electric fields produced by applying a voltage to an electrode. As a prototypical example, let us consider the Wiley-Maclauren spectrometer. The negative ions are accelerated by a Wiley-Maclauren spectrometer, and separated by time-of-flight. In essence, the Wiley-Maclauren spectrometer is a parallel plate capacitor that accelerates charged particles proportional to their charge to

mass ratio. As they fly, undesirable q/m particles can be deflected electrostatically, e.g., via quadrupole deflector or simple plate deflectors, before they enter the trap. Chromatographically separate by time-of-flight.

4.1.2 MCP

Charged semiconductor with diagonal holes. Charged species crash into hole wall, eject ions, get accelerated, crash into wall again and so forth, multiplying single anions to appreciable currents. Integrate peaks on detector to determine number.

4.2 Multipole Trap and Cooling

D^- is produced in a plasma discharge, and separated chromatographically using the Wiley-Maclauren spectrometer before loading into the MP trap.

Trap is probably loaded axially then static field to trap. Assuming that the apparatus used is an upgraded version of the one used in [9].

Once loaded into the trap, cooling has to be done by thermalization with the container walls via a buffer gas. This is because neither D^- nor H_2 have accessible transitions for optical cooling. The buffer gas cooling is most effective at high multipole order because the RF heating of the ion by the alternating electric field is limited to a narrow, sharp region at the boundary, rather than a broad shallow field over the entire trap. The temperature is not measured directly, but inferred based on a combination of thermalization with the known copper housing.

A buffer gas of H_2 is used. While hot D^- will react with the H_2 buffer gas, enough is cooled down quickly enough where an appreciable amount can build up in the trap. To monitor the trap population, a small voltage is used to kick a small piece of the ion cloud out of the trap.

Of course, at the beginning of cooling, there will be enough thermal energy to overcome the reaction barrier leading to a small initial H^- peak. However, Once cooled though, the amount of buffer gas is quite low so continued reaction rates are negligible. A portion of the cloud can be extracted from the trap and sent into another ToF spectrometer, with a MCP detector. Integrated current gives population.

Calibrated against typical loss rates. MP traps have to satisfy an adiabaticity condition, but collisions with buffer gas and other dynamical properties cause loss of all anionic species. This is measured and calibrated.

4.3 Reaction, Detection and Measurement

Then pump with H_2 to reaction concentration and allow to react at constant pressure for pseudo-first-order reaction. Fixed time, pressure, then pump down to not overwhelm MCP.

The detector is an MCP, a type of secondary emission multiplier, where a charged particle collides with a substrate, ejects more charged particles, and those charged particles are accelerated into another substrate, leading to a cascade of charged particles that can be detected as a current.

Naturally, such a detection is highly sensitive to the number of gas molecules, as the high voltages used to accelerate ions in the MCP can easily ionize the molecular hydrogen and overwhelm the detector. Thus, before measurements, the chambre is pumped down to a low H_2 pressure. Then, a small amount of the trapped ions is “kicked” from the multipole trap with a deflector electrode, accelerated by another WM spectrometer, and separated by ToF before measurement by the MCP. The current can be integrated to compare the fraction of ions that are hydrogen to deuterium.

Then, from this fraction, loss rates can be determined. Assuming particles have a fixed probability of leaving the trap, the rate of change in particle number of each species can be written

$$\frac{dH}{dt} = kD - x_H H \quad (5a)$$

$$\frac{dD}{dt} = -(k + x_D)D \quad (5b)$$

or

$$\frac{d}{dt} \begin{pmatrix} H \\ D \end{pmatrix} = \begin{pmatrix} -x_H & k \\ 0 & -(k + x_D) \end{pmatrix} \begin{pmatrix} H \\ D \end{pmatrix} \quad (6)$$

which has two eigenvectors,

$$\begin{pmatrix} H \\ D \end{pmatrix} = \begin{pmatrix} 1 \\ 0 \end{pmatrix}, \begin{pmatrix} -\frac{k}{k+x_D-x_H} \\ 1 \end{pmatrix} = V, U$$

with time evolutions

$$V = V_0 e^{-k_H t}$$

$$U = U_0 e^{-(k+x_D)t}$$

Therefore, the initial condition of (H_0, D_0) gives $U_0 = D_0$, $V_0 = \frac{k}{k+x_D-x_H} D_0 + H_0$, which evolves as

$$\frac{H}{D_0} = -\frac{k}{k+x_D-x_H} (e^{-(k+x_D)t} - e^{-x_H t}) + \frac{H_0}{D_0} e^{-x_H t} \quad (7a)$$

5 Results

Good agreement with predictions but only one data point, should better map out phase space

6 Figures

References

- [1] P. J. E. Peebles and R. H. Dicke, The Astrophysical Journal **154**, 891 (1968), Publisher: IOP ADS Bibcode: 1968ApJ...154..891P.
- [2] M. R. Krumholz, Notes on Star Formation, 2016, arXiv:1511.03457 [astro-ph].
- [3] N. Douguet *et al.*, Phys. Rev. A **88**, 052710 (2013), Publisher: American Physical Society.
- [4] A. G. G. M. Tielens, Rev. Mod. Phys. **85**, 1021 (2013), Publisher: American Physical Society.
- [5] M. Ayouz, R. Lopes, M. Raoult, O. Dulieu, and V. Kokoouline, Phys. Rev. A **83**, 052712 (2011), Publisher: American Physical Society.
- [6] W. Wang *et al.*, Chemical Physics Letters **377**, 512 (2003).
- [7] M. Zimmer and F. Linder, J. Phys. B: At. Mol. Opt. Phys. **28**, 2671 (1995).
- [8] E. S. Endres, O. Lakhmanskaya, M. Simpson, S. Spieler, and R. Wester, Phys. Rev. A **95**, 022706 (2017), Publisher: American Physical Society.
- [9] J. Mikosch *et al.*, Phys. Rev. A **78**, 023402 (2008), Publisher: American Physical Society.
- [10] D. Gerlich, Inhomogeneous RF Fields: A Versatile Tool for the Study of Processes with Slow Ions, in *Advances in Chemical Physics*, pp. 1–176, John Wiley & Sons, Ltd, 1992, _eprint: <https://onlinelibrary.wiley.com/doi/pdf/10.1002/9780470141397.ch1>.

A Dipole Approximation

Recall that a charged particle in an electromagnetic field has the hamiltonian

$$H = \frac{(\mathbf{p} - \frac{q}{c}\mathbf{A})^2}{2m} + qV \quad (8)$$

Fixing Coulomb gauge, $\nabla \cdot \mathbf{A} = 0$, we can expand about a small perturbing vector potential,

$$H = -\frac{\hbar^2 \nabla^2}{2m} + qV + \frac{i\hbar q}{mc} \mathbf{A} \cdot \nabla \quad (9)$$

with $\nabla^2 V(\mathbf{r}) = -4\pi\rho(\mathbf{r})$. Under the Coulomb gauge, solutions are given

$$\mathbf{A} = A\hat{\mathbf{e}}e^{i(\mathbf{k}\cdot\mathbf{r}-\omega t)} \quad (10)$$

which are exactly planewave, or polarized beams of light. In particular, in terms of the spectral intensity

$$I(\omega) = \frac{\omega^2}{2\pi c} |A|^2 \quad (11)$$

we can simplify the expansion of Fermi's Golden Rule

$$R = \frac{2\pi}{\hbar} \rho_f(E_f) |\langle f|V_1|i\rangle|^2 \quad (12)$$

as

$$R = \frac{4\pi^2 e^2}{m^2 c \omega^2} I(\omega) \begin{cases} \left| \int d^3r \psi_f^* e^{i\mathbf{k}\cdot\mathbf{r}} \hat{\mathbf{e}} \cdot \nabla \psi_i \right|^2 & \omega = +\omega_{fi} & \text{absorption} \\ \left| \int d^3r \psi_f^* e^{-i\mathbf{k}\cdot\mathbf{r}} \hat{\mathbf{e}} \cdot \nabla \psi_i \right|^2 & \omega = -\omega_{fi} & \text{emission} \end{cases} \quad (13)$$

Typically, we will have $\lambda \gg R_{\text{atom}}$, and so we can approximate $\mathbf{k} \cdot \mathbf{r} \sim R_{\text{atom}}/\lambda \ll 1$. The leading orders are the *dipole* and *quadrupole* operators

$$e^{\pm i\mathbf{k}\cdot\mathbf{r}} \approx 1 + i\mathbf{k} \cdot \mathbf{r} + \mathcal{O}[(\mathbf{k} \cdot \mathbf{r})^2]$$

Using

$$[\mathbf{r}, H_0] = \frac{i\hbar}{m} \mathbf{p}$$

we can write

$$\langle f|\hat{\mathbf{e}} \cdot \nabla|i\rangle = -\frac{m\omega_{fi}}{\hbar} \langle f|\hat{\mathbf{e}} \cdot \mathbf{r}|i\rangle \quad (14)$$

to obtain selection rules.

In particular, we consider this in two scenarios

A.1 Central Potentials

This scenario captures selection rules such as atomic transitions. We can rewrite

$$\hat{\epsilon} \cdot \mathbf{r} = \sqrt{\frac{4\pi}{3}} \left(\epsilon_x Y_{10} + \frac{-\epsilon_x + i\epsilon_y}{\sqrt{2}} Y_{11} + \frac{\epsilon_x + i\epsilon_y}{\sqrt{2}} Y_{1,-1} \right) \quad (15)$$

Naturally, we can use Clebsh-Gordon coefficients for the angular part of the transition

$$\langle \ell' m' | \hat{\epsilon} \cdot \mathbf{r} | \ell m \rangle \sim \int d\Omega Y_{\ell' m'}^* Y_{1q} Y_{\ell m} = \sqrt{\frac{3}{4\pi} \frac{2\ell+1}{2\ell'+1}} C_{\ell m 1q}^{\ell' m'} C_{\ell 0 10}^{\ell' 0} \quad (16)$$

which forces the selection rules

$$\Delta\ell = \pm 1 \quad (17a) \quad \Delta m = 0, \pm 1 \quad (17b)$$

There are additional constraints from the radial part of the overlap

$$\langle n' \ell' | \hat{\epsilon} \cdot \mathbf{r} | n \ell \rangle \sim \int dr r^3 R_{n' \ell'}^* R_{n \ell} \quad (18)$$

which, for example, enforce a parity change.

Note, that a rigid rotor is a central potential in CoM coordinates.

A.2 Harmonic Oscillator

Substitute \mathbf{r} with the quantization axis as $\mathbf{r} \sim (a^\dagger + a)\hat{x}$. Then, the selection rules become

$$\Delta n = \pm 1 \quad (19a) \quad \hat{\epsilon} \not\perp \hat{x} \quad (19b)$$

Anharmonicity adds terms $\sim x^n \sim (a^\dagger + a)^n$ which lead to additional *overtones*

A.3 Vibrotational

To second order in the quantum numbers ν, ℓ , the harmonic oscillator gains an anharmonic correction

$$H_{AHO} = \hbar\omega_e \left(\nu + \frac{1}{2} \right) - \omega_e \chi_e \left(\nu + \frac{1}{2} \right)^2$$

the rigid rotor gains centrifugal distortion term

$$H_{NRR} = B_e \ell(\ell+1) + D_e [\ell(\ell+1)]^2$$

and a vibrotational coupling is added

$$H_{RV} = -hc\alpha_e \left(\nu + \frac{1}{2} \right) [\ell(\ell+1)]$$

This is of course much more difficult to treat analytically, but if we treat these as perturbations about H_{SHO} and H_{RR} , we can inherit those selection rules.

A.4 FTIR vs Raman

FTIR probes the leading order dipole coupling, while Raman, as a virtual process involving two photons, probes quadrupole couplings.

B Star formation

Star formation requires gravitational and external pressures to overcome internal energies and pressures. This can be stated[2]¹ as the *virial equation*

$$\begin{aligned}
\ddot{I} = & \int_V dV \left(\frac{1}{2} \rho v^2 + \frac{3}{2} P \right) \\
& + \int_{\partial V} r^i \Pi_{ij} dS^j \\
& + \frac{1}{8\pi} \int_V B^2 dV + \int_{\partial S} r^i T_{ij} dS^j \\
& - \int_V dV \rho \mathbf{r} \cdot \nabla \phi \\
& - \frac{1}{2} \int_{\partial V} \rho r^2 \mathbf{v} \cdot d\mathbf{S}
\end{aligned} \tag{20}$$

where the first line \mathcal{T} are the kinetic and thermal energy, the second line \mathcal{T}_S is the confining pressure $\Pi_{ij} = \rho v_i v_j + P \delta_{ij}$ from ram and thermal pressure respectively, the third line \mathcal{B} is the difference between the internal magnetic pressure and the external magnetic pressure/tension from the Maxwell stress tensor T_{ij} , the fourth line \mathcal{W} is the energy due to the gravitational potential ϕ , and the final term is the rate of change of the momentum flux. If magnetic and surface effects are negligible and the system is in hydrostatic equilibrium, we obtain a virial ratio

$$\alpha_{\text{virial}} = \frac{2T}{|W|} \tag{21}$$

where for $\alpha_{\text{virial}} > 1$ implies $\ddot{I} > 0$ and vice-versa. If there is only thermal pressure,

$$\mathcal{T} \approx \frac{3}{2} M c_s^2 \quad \mathcal{W} \approx -a \frac{GM^2}{R}$$

this leads to the *Jeans criterion*

$$R \gtrsim \frac{c_s}{\sqrt{G\rho}} \tag{22}$$

for a stable gas cloud. If this is violated, the cloud begins to collapse. More rigorous linearized perturbation of the hydrodynamics and self gravity determine a dispersion relationship

$$\omega^2 = c_s^2 k^2 - 4\pi G \rho_0 \tag{23}$$

¹derived from MHD

which at $\omega = 0$ yields a critical point

$$\lambda_J = \frac{2\pi}{k} = \sqrt{\frac{\pi c_s^2}{G\rho_0}} \quad (24)$$

above which perturbations grow exponentially, and below which perturbations are stabilized. In particular, the dispersion relation gives a timescale of freefall, $\tau \sim 1/|i\omega|$.

B.1 Early Stars

In order to reduce \mathcal{T} to allow star formation, the early gas clouds had to cool. However, these clouds were comprised mostly of ^1_1H and ^4_2He , whose atomic transitions occurred at roughly $10\text{ eV} \sim 10^5\text{ K}$; below this temperature, atomic lines are inefficient at cooling. The $J = 2$ transition of molecular H_2 has a characteristic temperature of about 500 K , and can cool to about 200 K . This phase is the *loitering phase*, but as the region at 200 K grows larger, the rate of three body recombination increases, allowing for the density to increase until an equilibrium between the heating from binding energy release competes with cooling from quadrupole line emission. Eventually, the density increases to the point where they are thick to the H_2 lines, so heating dominates, and the star can begin collapsing/fusing.

C RF Traps

This section primarily follows [10]. Recall the Lorentz force,

$$m\ddot{\mathbf{r}} = q\mathbf{E} + q\dot{\mathbf{r}} \times \mathbf{B} \quad (25)$$

For cryogenic temperatures, i.e. slow atoms, the effect due to the magnetic field is going to be heavily suppressed by the magnitude of $\dot{\mathbf{r}}$, so it is neglected. The electric field can be engineered such that it can be separated into an RF and a DC component.

$$\mathbf{E}(\mathbf{r}, t) = \mathbf{E}_{RF}(\mathbf{r}) \cos \Omega t + q\mathbf{E}_{DC}(\mathbf{r}) \quad (26)$$

For convenience, we fix $\mathbf{E}_{DC} = 0$, although it will be used later to create an axial confinement. Additionally we treat inhomogeneities in the RF fields as perturbations to a homogeneous field,

$$\mathbf{E}_{RF}(\mathbf{r}) = \mathbf{E}_0 + \mathbf{E}_I(\mathbf{r}) \quad \mathbf{E}_I(0) = 0 \quad (27)$$

In particular, a solution to the homogeneous field can be trivially found by integration

$$\mathbf{R}_{RF}(t) = -\frac{q\mathbf{E}_0}{m\Omega^2} \cos \Omega t \equiv -\mathbf{a} \cos \Omega t \quad (28)$$

Note that the amplitude of oscillations is suppressed by the frequency of the RF trap. By choosing a relatively high frequency, we can treat the oscillations due to the homogeneous

field as a small perturbation superposed on top of the drift due to a weak or slowly varying inhomogeneous field,

$$\mathbf{r}(t) = \mathbf{R}_d(t) + \mathbf{R}_{\text{RF}}(t) \quad (29)$$

thus, we can expand the electric field the particle feels as a function of time

$$\mathbf{E}_{\text{RF}}(\mathbf{r}(t)) \approx \mathbf{E}_{\text{RF}}(0) - (\mathbf{a} \cdot \nabla) \mathbf{E}_{\text{RF}}(0) \cos \Omega t + \mathcal{O}(E_I^2)$$

Since the drift velocity is small and the field inhomogeneities are small, we additionally have $\dot{\mathbf{a}} \ll \Omega a$, $\dot{\mathbf{R}}_d \ll \Omega \mathbf{R}_d$. After substituting, neglecting small terms, and applying the identity

$$(\mathbf{v} \cdot \nabla) \mathbf{v} = \frac{1}{2} \nabla v^2 - \mathbf{v} \times (\nabla \times \mathbf{v})$$

the drift EoM becomes

$$m \ddot{\mathbf{R}}_d = -\frac{q^2}{4m\Omega} \nabla E_{\text{RF}}^2 \quad (30)$$

Naturally, as $\mathbf{F} = -\nabla U$, we can write an effective potential

$$U_{\text{eff}} = \frac{q^2}{4m\Omega} E_{\text{RF}}^2 + q\Phi$$

We obtain an interpretation that particles tend to drift towards regions with lower field amplitudes. A natural implementation of such a field configuration is the multipole trap

C.1 Multipole Configuration

Solving Laplace's equation, an ideal multipole configuration located at radius r_0 and having a profile $\Phi_n(r_0, \varphi) = \cos n\varphi$, $\Phi_n(0) = 0$, will have a potential

$$\Phi_n(r, \varphi) = \Phi_0 \left(\frac{r}{r_0} \right)^n \cos n\varphi$$

yielding an effective potential